The phosphorylation of AMPKβ1 is critical for increasing autophagy and maintaining mitochondrial homeostasis in response to fatty acids

Eric M. Desjardins[a,b] (ID), Brennan K. Smith[a,b], Emily A. Day[a,b,1], Serge Ducommun[c,2] (ID), Matthew J. Sanders[c] (ID), Joshua P. Nederveen[a,d], Rebecca J. Ford[a,b], Stephen L. Pinkosky[a,b], Logan K. Townsend[a,b], Robert M. Gutgesell[a,b] (ID), Rachel Lu[a,b], Kei Sakamoto[c,e,3] (ID), and Gregory R. Steinberg[a,b,f,3] (ID)

Fatty acids are vital for the survival of eukaryotes, but when present in excess can have deleterious consequences. The AMP-activated protein kinase (AMPK) is an important regulator of multiple branches of metabolism. Studies in purified enzyme preparations and cultured cells have shown that AMPK is allosterically activated by small molecules as well as fatty acyl-CoAs through a mechanism involving Ser108 within the regulatory AMPK β1 isoform. However, the in vivo physiological significance of this residue has not been evaluated. In the current study, we generated mice with a targeted germline knock-in (KI) mutation of AMPKβ1 Ser108 to Ala (S108A-KI), which renders the site phospho-deficient. S108A-KI mice had reduced AMPK activity (50 to 75%) in the liver but not in the skeletal muscle. On a chow diet, S108A-KI mice had impairments in exogenous lipid-induced fatty acid oxidation. Studies in mice fed a high-fat diet found that S108A-KI mice had a tendency for greater glucose intolerance and elevated liver triglycerides. Consistent with increased liver triglycerides, livers of S108A-KI mice had reductions in mitochondrial content and respiration that were accompanied by enlarged mitochondria, suggestive of impairments in mitophagy. Subsequent studies in primary hepatocytes found that S108A-KI mice had reductions in palmitate- stimulated Cpt1a and Ppargc1a mRNA, ULK1 phosphorylation and autophagic/mitophagic flux. These data demonstrate an important physiological role of AMPKβ1 Ser108 phosphorylation in promoting fatty acid oxidation, mitochondrial biogenesis and autophagy under conditions of high lipid availability. As both ketogenic diets and intermittent fasting increase circulating free fatty acid levels, AMPK activity, mitochondrial biogenesis, and mitophagy, these data suggest a potential unifying mechanism which may be important in mediating these effects.

AMPK | fat oxidation | mitochondria | NAFLD | autophagy

Fatty acids are a predominant substrate for most cell types and also act as critical building blocks for membranes and signaling molecules. However, high levels of fatty acids –common in obesity– promote the development of lipotoxicity in multiple organ systems, triggering inflammation, fibrosis, and eventually cell death (1). As such, multiple homeostatic mechanisms have evolved to closely match fatty acid availability with oxidation rates. This includes allosteric inhibition of key enzymes regulating fatty acid oxidation including acetyl-CoA carboxylase (ACC) (2). Fatty acids can also increase their own oxidation by enhancing mitochondrial function through the coordinated regulation of mitochondrial biogenesis and degradation (3–5). However, to date, the mechanisms coordinating the effects of fatty acids on mitochondrial homeostasis are incompletely understood.

The AMP-activated protein kinase (AMPK) is a central governor of cellular energy homeostasis that is influenced by multiple physiological, hormonal, and nutritional signals. AMPK is a heterotrimeric protein consisting of a catalytic α (α1/α2) subunit, a regulatory γ (γ1/γ2/γ3) subunit, and a β (β1/β2) subunit, which is critical for both maintaining the structure of the enzyme complex and regulating enzyme activity (6). Studies in knock-out mice have shown that AMPKβ1 is essential for maintaining AMPK activity in metabolic tissues such as the liver (7), while AMPKβ2 is important in the skeletal muscle and heart (8). In addition to acting as a structural scaffold, the β subunit is also (auto)phosphorylated and myristoylated to allosterically regulate enzymatic activity (9–13). Of these posttranslational modifications, phosphorylation of AMPKβ1 Ser108 has been shown to play a vital role in enhancing AMPK activity in response to many distinct, small-molecule, allosteric activators including A769662, salicylate, 991, MK-8722, PF-06409577, and lusianthridin (14–20) (reviewed in ref. 6). And, while the endogenous ligand(s) for β1 Ser108 remained elusive for many years, recent studies conducted in cultured cells and purified enzyme preparations identified that long-chain fatty acyl-CoAs increase AMPK

Significance

The data in this manuscript indicate a crucial role for a single phosphorylation site on the regulatory beta subunit of AMPK to stimulate mitochondrial biogenesis and autophagy/ mitophagy in response to increases in fatty acids. This suggests a potential unifying mechanism which may be important for mediating the beneficial effects of dietary interventions that increase free-fatty acid availability such as intermittent fasting and ketogenic diets.

activity in part through this residue (2). Ser108 is also phosphorylated by the autophagy initiator Unc-51-like kinase 1 (ULK1) (12). Despite the growing appreciation of this posttranslational modification, little is known about the physiological importance of AMPKβ1 Ser108, information that is especially relevant given new small molecules that activate AMPK through this residue have entered clinical trials for nonalcoholic steatohepatitis (21, 22) and may be potentially utilized for other chronic diseases.

Results

We find that, consistent with previous studies in cell-free assays (12, 15–17), β1 S108A-containing AMPK trimeric complexes were not responsive to A769662-mediated activation but were sensitive to phosphorylation by Ca^{2+}/calmodulin-dependent protein kinase kinase-β (CaMKKβ) and allosteric activation by AMP (*SI Appendix*, Fig. S1). To investigate the physiological importance of AMPKβ1 Ser108 phosphorylation, we generated a mouse model with a targeted germline knock-in (KI) mutation in which this residue was rendered phospho-deficient by mutating the Ser to Ala (S108A-KI) (*SI Appendix*, Fig. S2).

In mice fed a control high-carbohydrate chow diet (CD), S108A-KI mice had lower AMPK activity in the liver but not in the skeletal muscle (Fig. 1A), a finding consistent with the predominant expression of the AMPKβ1 subunit in the liver but not in the skeletal muscle (*SI Appendix*, Fig. S3A). Importantly, this lower AMPK activity was independent of observable changes in the expression of AMPK α, β, or γ isoforms (*SI Appendix*, Fig. S3A). We subsequently examined body mass, energy expenditure, fasting blood glucose, caloric consumption, physical activity levels, the respiratory exchange ratio (RER), and glucose tolerance and found that there were no genotypic differences in these parameters (*SI Appendix*, Fig. S3 *B–H*). These data indicate that on a control

chow diet S108A-KI mice have reductions in AMPK activity within the liver that are independent of changes in AMPK isoform expression profiles, but that this does not have a significant impact on whole-body glucose homeostasis or energy balance.

Given previous studies in purified enzyme preparations found that AMPKβ1 Ser108 was important for activating AMPK in response to increases in fatty acyl-CoA availability (2), we next challenged WT and S108A-KI mice fed a control chow diet with an oral bolus of the lipid emulsion intralipid (Fig. 1B). Food intake (*SI Appendix*, Fig. S4A) and activity levels (*SI Appendix*, Fig. S4B) were not different between genotypes or following intralipid gavage. Compared to vehicle control, there was a tendency for intralipid gavage to reduce the RER in WT ($P = 0.2$, *SI Appendix*, Fig. S4 *C and E*) but not S108A-KI ($P = 0.9$, *SI Appendix*, Fig. S4 *D and E*) mice, and when changes in fatty acid oxidation were calculated, this was increased by intralipid in WT but not in S108A-KI mice (Fig. 1C). In contrast, treatment of WT and S108A-KI mice with 5-aminoimidazole-4-carboxamide-1-β-D-ribofuranoside (AICAR)–which is metabolized into the AMP-mimetic (ZMP or AICAR monophosphate) and activates AMPK via the γ not the β1 isoform (23)–did not change food intake or activity (*SI Appendix*, Fig. S4 *F and G*), but reduced RER (*SI Appendix*, Fig. S4 *H–J*) and increased fatty acid oxidation in both genotypes (Fig. 1D).

AMPK phosphorylation of ACC is important for increasing fatty acid oxidation in response to intralipid (2). Consistent with these previous findings, treatment of primary hepatocytes with palmitate increased ACC1/2 S79/212 phosphorylation in WT mice but not in S108A-KI mice (Fig. 1E), while the effect of AICAR was maintained in both genotypes (Fig. 1F). Similar to palmitate, S108A-KI mice were also resistant to the effects of A769662 to increase ACC phosphorylation (Fig. 1G). These findings demonstrate that AMPKβ1 Ser108 is important for increasing
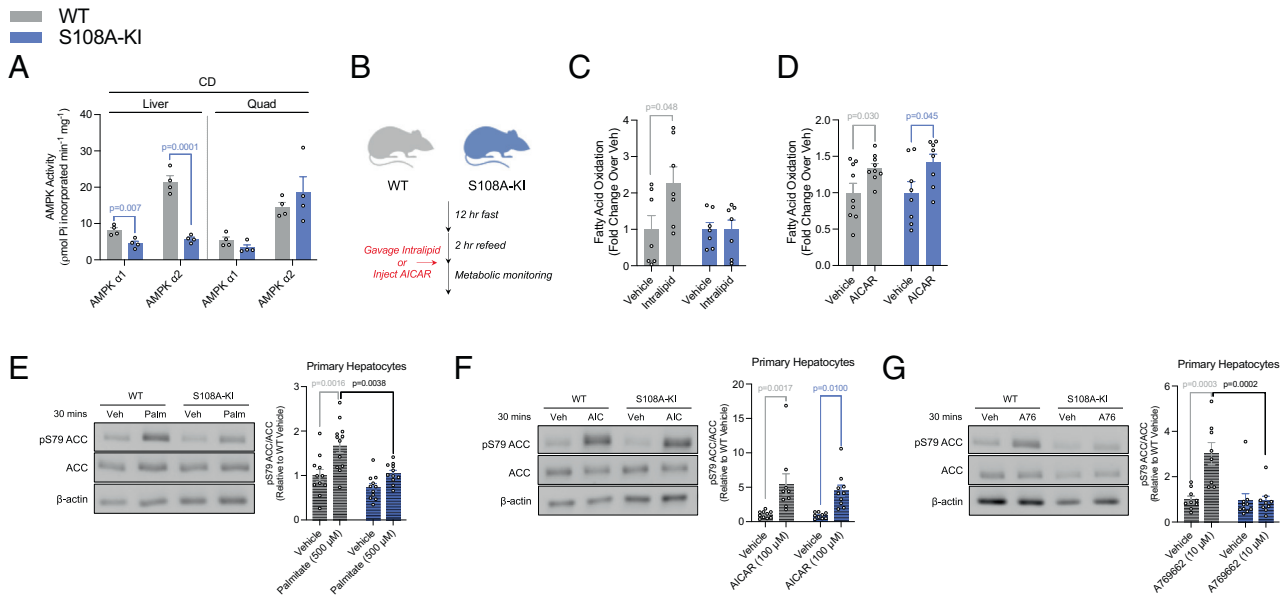

Fig. 1. AMPKβ1 Ser108 phosphorylation is important for acute fatty acid-induced increases in ACC phosphorylation and whole-body fatty acid oxidation. (*A*) AMPKα isoform-specific phosphotransferase activity assay from basal chow-fed (CD) WT and S108A-KI (KI) mice for liver and quadriceps muscle (Quad). (*B–D*) Schematic of fast-refeed experiments with or without intralipid or AICAR in metabolic monitoring units (*B*). Fatty acid oxidation (*C*) was calculated from VO_2 and VCO_2 over 4 h, starting 1 h postgavage of either saline or 20% intralipid (10 mL/kg) in WT and S108A-KI mice fed a chow diet. Following an i.p. injection of saline or AICAR (500 mg/kg), fatty acid oxidation (*D*) was calculated from VO_2 and VCO_2 over 1 h, starting 6 h postinjection. Representative ACC immunoblotting and densitometrical analysis assessing inhibitory phosphorylation of ACC by AMPK in response to palmitate (Palm: 500 μM) (*E*), AICAR (AIC: 100 μM) (*F*), and A-769662 (A76: 10 μM) (*G*) in primary hepatocytes from CD-fed WT and S108A-KI mice. Data are means ± SEM with *P*-values reported in the graphs. Gray bars equal WT differences, blue bars equal to S108A-KI differences, and black bars indicate differences between groups in same treatment condition. Statistical significance was accepted at $P < 0.05$ and determined via multiple *t* tests or two-way ANOVA with Tukey's posthoc analysis. White circles are individual mice or experimental replicates with three technical replicates per group.

the phosphorylation of ACC in response to acute increases in free fatty acids, but not AMP-mimetics such as AICAR.

To examine the chronic consequences of elevations in free fatty acids, WT and S108A-KI mice were fed a high-fat diet (HFD). Although we could not perform densitometrical analyses reliably due to a low-molecular-weight nonspecific band, compared to chow-fed controls, HFD feeding seemed to increase AMPKβ1 Ser108 phosphorylation in the liver of WT mice, while, as expected, this signal was undetectable in S108A-KI mice (Fig. 2A). However, we did not detect a significant reduction in ACC phosphorylation as total ACC protein content was markedly reduced in HFD compared to chow-fed controls (Fig. 2 A–C). Body mass, energy expenditure, fasting blood glucose, caloric intake, and physical activity levels were similar between WT and S108A-KI mice fed a HFD (*SI Appendix*, Fig. S3 B–G). In contrast to the acute increase in free fatty acid availability induced by intralipid gavage (Fig. 1), there was no difference in RER between WT and S108A-KI mice fed a HFD (*SI Appendix*, Fig. S3G). This finding is consistent with the comparably large reductions in ACC expression elicited by the HFD in both WT and S108A-KI mice and previous observations that ACC S79/S212A (ACC-DKI, (24)) mice have normal increases in fatty acid oxidation (i.e., reductions in RER) in response to a HFD. HFD-fed S108A-KI mice had a tendency for modest impairments in glucose tolerance (Fig. 2D). This tendency for reduced glucose tolerance was not associated with differences in insulin levels which were similar between HFD-fed WT and S108A-KI mice at 2- and 10-min post glucose injection (Fig. 2E), suggesting that S108A-KI mice had impaired insulin sensitivity. As hepatic steatosis contributes to insulin resistance, we examined liver lipids and found that S108A-KI mice had increased steatosis and an ~10% increase in liver triglycerides compared to WT controls fed a HFD (Fig. 2 F and G).

In addition to acutely stimulating fatty acid oxidation through phosphorylation of ACC (24), AMPK may chronically increase fatty acid oxidation by enhancing mitochondrial function through the coordinated regulation of mitochondrial biogenesis, mitophagy, and mitochondrial fission (25, 26). Under conditions of a HFD, S108A-KI mice had lower protein abundance of the electron transport chain complexes 2-5 in the liver (Fig. 2H), effects not observed in animals fed a chow diet (*SI Appendix*, Fig. S3I). HFD-fed S108A-KI mice also had reduced mRNA expression of *Ppargc1a* (Fig. 2I). Furthermore, when treated with palmitate for 6 h, primary hepatocytes from S108A-KI mice had an attenuated induction in the mRNA expression of both *Cpt1a* and *Ppargc1a* (Fig. 2 J–L). These data indicate that AMPKβ1 Ser108 is important for increasing mitochondrial biogenesis in response to chronic increases in fatty acid availability.

To examine whether there might be changes in mitochondrial function independently of reductions in mitochondrial content, we measured respiration in isolated liver mitochondria from chow- and HFD-fed mice. In mice fed a HFD, succinate-stimulated respiration was increased in WT mice but not in S108A-KI mitochondria (Fig. 3A). Reduced rates of respiration per mitochondrial mass led us to examine mitochondrial morphology by transmission electron microscopy (TEM), where it was observed that the average surface area of liver mitochondria from HFD-fed S108A-KI mice was increased (Fig. 3 B and C), while there was a reduced number of mitochondria (Fig. 3 B and D). Taking these two measurements into consideration, we calculated the average mitochondrial surface area per field and found that HFD-fed S108A-KI mice had a greater mitochondrial area per micrograph compared to WT mice (Fig. 3 B and E). Enlarged and dysfunctional mitochondria are hallmarks of impaired autophagy and have been observed in other models of AMPK deficiency as well as in people with NAFLD (25, 27). Therefore, we investigated
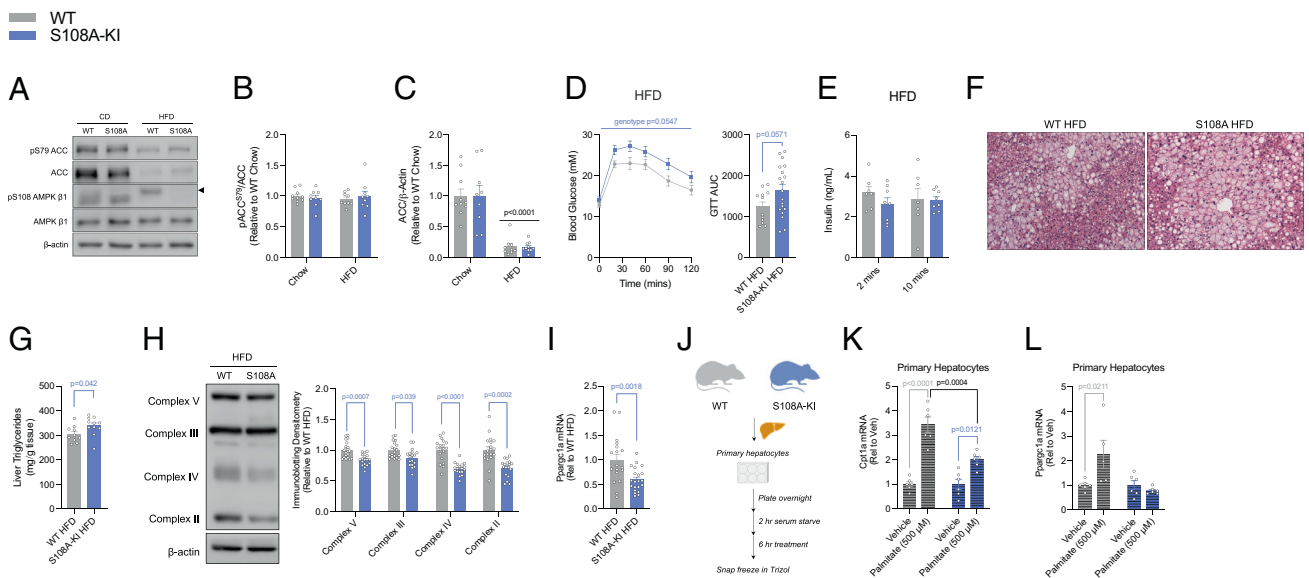

Fig. 2. AMPKβ1 Ser108 phosphorylation is important for increasing mitochondrial biogenesis in mice fed a HFD or hepatocytes treated with palmitate. (*A*) Representative immunoblots of ACC1/2 S79/S212 and AMPKβ1 S108 and densitometrical analysis of pACC/ACC (*B*) and total ACC (*C*) from the livers of chow-fed (CD) and HFD-fed (HFD) WT and S108A-KI mice. (*D*) Intraperitoneal glucose tolerance test (Intraperitoneal glucose tolerance tests (ipGTT), 0.8 g/kg) and area under the curve (GTT AUC) at 24 wk of age in HFD-fed WT and S108A-KI mice. (*E*) Serum insulin at 2- and 10-min post glucose injection from some of the mice in *D* in which blood samples could be collected. Representative H&E stains (10×, *F*) and liver triglycerides (*G*) of WT and S108A-KI mice fed a HFD for 20 wk. Representative immunoblots and densitometrical analysis of OXPHOS complexes 2-5 of WT and S108A-KI mice fed a HFD (*H*). mRNA expression of peroxisomeproliferator activated receptor gamma coactivator 1-alpha (*Ppargc1a*) in WT and S108A-KI mice fed a HFD (*I*). (*J–L*) Schematic representation of mRNA experiments in primary hepatocytes for mitochondrial biogenesis in response to elevated LCFAs (*J*). Carnitine-palmitoyl transferase 1-alpha (*Cpt1a*) (*K*) and *Ppargc1a* (*L*) mRNA expression from primary hepatocytes. Data are means ± SEM with *P*-values reported in the graphs. Gray bars equal WT differences, blue bars equal to S108A-KI differences, and black bars indicate differences between groups in same treatment condition. Significance was accepted at *P* < 0.05 and determined via *t* tests, ordinary two-way, or repeated-measures two-way ANOVA with Tukey's posthoc analysis, where appropriate. White circles are individual mice per group. Black arrow in *A* indicates area for specific band of AMPKβ1 S108.
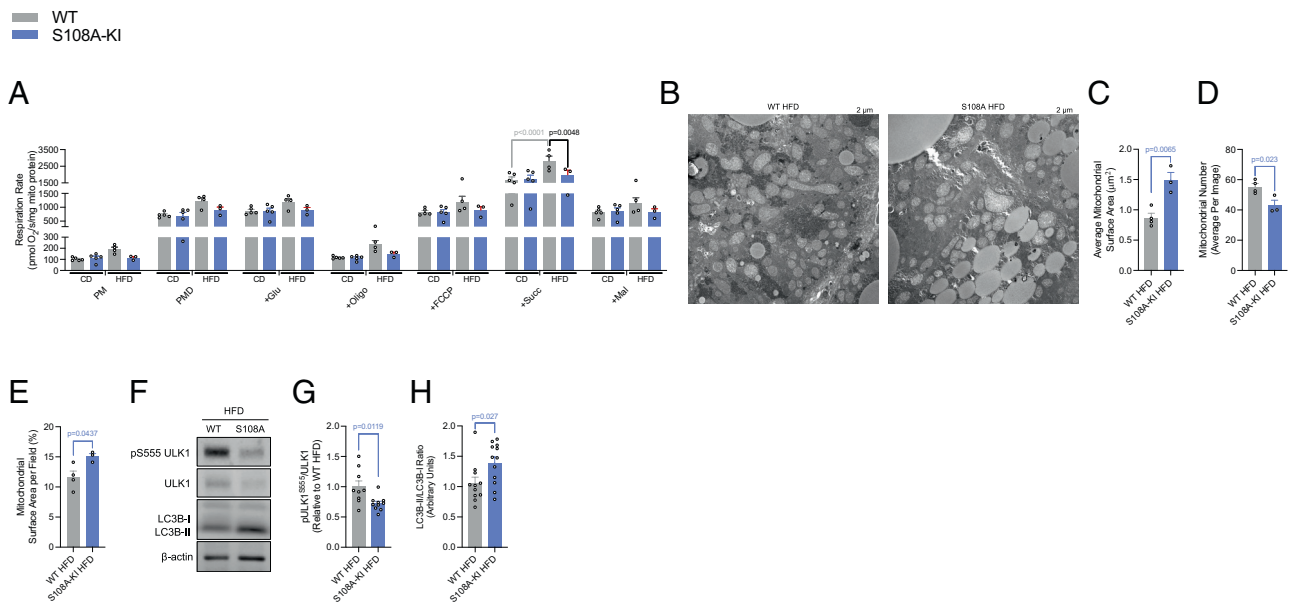
Fig. 3. AMPKβ1 Ser108 phosphorylation is important for increasing ULK1 phosphorylation and maintaining mitochondrial morphology and function in response to a HFD. Respiration rates (*A*) from isolated liver mitochondria from CD and HFD-fed WT and S108A-KI mice (PM; 0.5 mM malate, 5 mM pyruvate, PMD; + 1 mM ADP, +Glu; 5 mM glutamate, +Oligo; 1.25 μM oligomycin, +FCCP; titration of 0.5 μM FCCP until maximal uncoupled respiration reached, +Succ; 10 mM succinate, and +Mal; 5 mM malonate). Representative electron micrographs (*B*) with quantification of average mitochondrial surface area (*C*), mitochondrial number (*D*), and mitochondrial surface area per field (*E*) from WT and S108A-KI mice fed a HFD. Representative immunoblotting (*F*) and densitometrical analysis of pULK S555/ULK1 (*G*) and LC3BII (*H*) from the livers of WT and S108A-KI mice fed a HFD. Data are means ± SEM with *P*-values reported in the graphs. Gray bars equal WT differences and blue bars equal to S108A-KI differences. Statistical significance was accepted at *P* < 0.05 and determined via unpaired *t* test, two-way ANOVA with Tukey's posthoc analysis, or repeated-measures two-way ANOVA with Sidak's posthoc analysis, where appropriate. White circles are individual mice or technical replicates from three experimental replicates per group.

whether this process was also dysregulated in the liver of the HFD-fed S108A-KI mice. We found that ULK1 S555 phosphorylation was reduced (Fig. 3 *F* and *G*), while the ratio of LC3B-II/LC3B-I was increased (Fig. 3 *F* and *H*) in S108A-KI mice fed a HFD. These data indicate that AMPKβ1 Ser108 is critical for maintaining ULK1 phosphorylation, mitochondrial function, and morphology in the liver when mice are fed a HFD.

Considering autophagy as an active process, we used primary hepatocytes to investigate the initiation and flux through the pathway due to excess palmitate (Fig. 4*A*). After 30 min of treatment with palmitate, primary hepatocytes from WT mice had increases in the phosphorylation of ULK1 S555, but this effect was not observed in S108A-KI mice (Fig. 4 *B* and *C*). Furthermore, the downstream substrate of ULK1, ATG14, had unaltered S29 phosphorylation by palmitate treatment in either group but was modestly reduced in hepatocytes from S108A-KI mice (Fig. 4 *B* and *D*). We subsequently assessed autophagic flux using the lysosomal pH neutralizing agent chloroquine and detected reduced palmitate-induced autophagic flux (chloroquine treated vs. untreated) in S108A-KI-derived hepatocytes in comparison to WT counterparts by measurements of LC3B-II levels (Fig. 4*E*). Similarly, under a more chronic condition, palmitate-induced autophagic flux was attenuated in S108A-KI hepatocytes transfected with a tandem fluorescent protein construct including an acid-sensitive GFP and an acid-insensitive RFP (Fig. 4 *F–H*). Last, to determine whether mitophagy was sensitive to palmitate and if this response was altered in S108A-KI hepatocytes, we isolated mitochondrially enriched extracts and found that mitochondrial LC3B-II levels were significantly higher in response to palmitate in WT versus S108A-KI hepatocytes (Fig. 4 *I–K*). Other markers of mitophagy including p62, BNIP3, NIX, and CISD1 did not show any differences in response to palmitate between groups (*SI Appendix*, Fig. S5 *A–E*). Taken together, these findings describe a critical role for an AMPK-fatty acid sensing axis for acutely

increasing fatty acid oxidation while chronically enhancing autophagy/mitophagy and mitochondrial biogenesis (Fig. 4*L*).

Discussion

Structural and cell-based studies have identified phosphorylation of Ser108 within the AMPKβ1 subunit as an important event for allosteric activation of AMPK in response to small molecules (15–17) and fatty acyl-CoA (2), but the in vivo physiological importance of this residue is unknown. In the current study, we find that in mice fed a control high-carbohydrate diet, there are reductions in liver AMPK activity in S108A-KI mice that occur independently of changes in AMPK subunit expression. This reduction in liver AMPK activity does not result in detectable changes in whole-body metabolic parameters or liver mitochondrial content and function. These findings are consistent with previous observations that phosphorylation of AMPKβ1 Ser108 is maintained at low levels in the basal state (28) and that small amounts of AMPK activity are sufficient to maintain metabolic homeostasis and mitochondrial function in the absence of a metabolic challenge. We find that acutely increasing free fatty acids through an oral gavage of intralipid and treating primary hepatocytes with palmitate promotes fatty acid oxidation and ACC phosphorylation, respectively, in WT mice but not in S108A-KI mice. This is in contrast to the effects of AICAR which stimulates fatty acid oxidation and ACC phosphorylation in both WT and S108A-KI mice to a comparable degree, highlighting the specificity of this response. These data, in combination with previous studies (2), support a model in which acute elevations in fatty acids promote fatty acid oxidation through: 1) interactions with Ser108 within the AMPKβ1 subunit; 2) allosteric activation of AMPK; 3) phosphorylation and inhibition of ACC; 4) reduced malonyl-CoA, relieving allosteric inhibition of carnitine palmitoyl-transferase 1 (CPT1); and 5) increased flux of fatty acyl-CoA
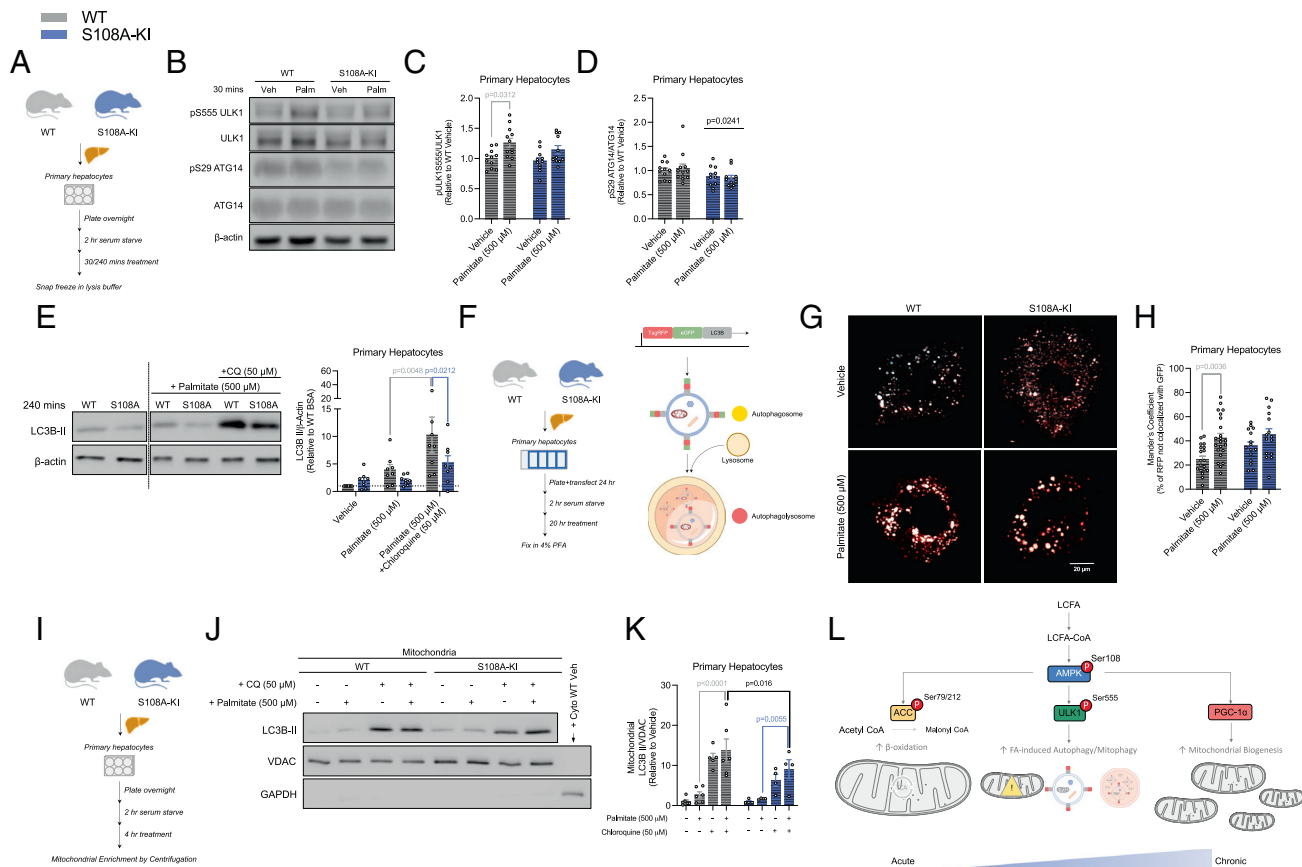
Fig. 4. AMPKβ1 Ser108 phosphorylation is important for increasing autophagy and mitophagy in response to increases in fatty acid availability. (*A–F*) Schematic of immunoblotting experiments for palmitate-induced autophagy and autophagic flux experiments in primary hepatocytes (*A*). Representative immunoblots (*B*) and densitometrical analysis of ULK1 (S555) (*C*) and ATG14 (S29) (*D*) assessing the induction of autophagy via AMPK activation in response to palmitate (500 μM) in primary hepatocytes from CD-fed WT and S108A-KI mice. Representative LC3B-II immunoblotting and densitometrical analysis (*E*) assessing autophagic flux in response to palmitate (500 μM) in primary hepatocytes from CD-fed WT and S108A-KI mice. (*F–H*) Schematic of palmitate-induced autophagic flux in primary hepatocyte experiments by tandem fluorescence and graphical illustrating result of using the LC3B protein with an acid-sensitive GFP and an acid-insensitive RFP (*F*). Representative colorblindness-friendly confocal micrographs with green being replaced with cyan (autophagosomes appear as white, while autophagolysosomes are red) (*G*), and quantification of percent red not overlapping green (*H*) in CD-fed WT and S108A-KI primary hepatocytes treated with vehicle or palmitate. (*I–K*) Schematic of immunoblotting experiments for palmitate-induced mitophagic flux experiments in primary hepatocytes (*I*). Representative immunoblotting (*J*) and densitometrical analysis of LC3B-II (*K*) assessing mitophagic flux in response to palmitate (500 μM) in primary hepatocytes from CD-fed WT and S108A-KI mice. Working model of the role of AMPKβ1 Ser108 phosphorylation in an AMPK-fatty acid-sensing axis to increase fatty acid oxidation, autophagy/mitophagy, and mitochondrial biogenesis (*L*). Data are means ± SEM with *P*-values reported in the graphs. Gray bars equal WT differences, blue bars equal to S108A-KI differences, and black bars indicate differences between groups in same treatment condition. A straight black line indicates a main effect of genotype in *D*. Statistical significance was accepted at *P* < 0.05 and determined via repeated-measures two-way ANOVA with Sidak's posthoc analysis, unpaired *t* tests, or two-way ANOVA with Tukey's posthoc analysis, where appropriate. White circles are individual mice or technical replicates from experiments with three experimental replicates per group. For confocal microscopy analysis, white circles represent individual micrographs from two experimental replicates per group.

into the mitochondria for β-oxidation. These data also suggest that allosteric inhibition of ACC is insufficient to enhance fatty acid oxidation in the absence of covalent regulation by AMPK.

We find that feeding mice a HFD increases AMPKβ1 Ser108 phosphorylation compared to chow-fed controls. This is not accompanied by reductions in ACC phosphorylation in S108A-KI mice fed a HFD and is consistent with studies in mice lacking inhibitory phosphorylation sites on ACC, which have comparable rates of fatty acid oxidation when fed a HFD (24). Furthermore, previous studies in obese mice with reductions in ACC expression have been linked to hyperleptinemia-induced activation of PPARα and subsequent reductions in SREBP1c (29). These data indicate that, in contrast to the acute increases in free fatty acid availability, chronic feeding of an obesity-promoting HFD enhances whole-body fatty acid oxidation independently of AMPKβ1 Ser108 phosphorylation.

In addition to modulating ACC, chronic exposure of fatty acids increases mitochondrial biogenesis (5, 30). Many genetic models of AMPK deficiency have a reduction in tissue mitochondrial content, while treatment of rodents with pharmacological activators

of AMPK stimulates mitochondrial biogenesis (31–34). We found that S108A-KI mice were resistant to the stimulatory effects of a HFD to increase mitochondrial content in the liver and were also resistant to the acute stimulatory effects of palmitate to increase *Cpt1a* and *Ppargc1a* in hepatocytes. These findings highlight an important role of AMPKβ1 Ser108 phosphorylation in enhancing mitochondrial biogenesis–an effect which may involve increases in PGC1α (reviewed in refs. 25 and 26). Supporting this concept, mice heterozygous for liver PGC1α that were fed a HFD had a very similar metabolic phenotype to S108A-KI mice, with reductions in mitochondrial beta-oxidation genes, hepatic steatosis, and glucose intolerance (35). These data are also consistent with observations in clinical populations, which indicate that modest reductions in maximal mitochondrial respiration can, over time, promote steatosis and insulin resistance (36).

Mitochondria isolated from the livers of S108A-KI mice had reductions in respiration in the setting of a HFD, indicating that there were also impairments in mitochondrial function that were independent of reductions in mitochondrial content. Subsequent analysis of mitochondrial morphology revealed large and distended

mitochondria within the liver of S108A-KI mice, a hallmark of impaired mitophagy. Many previous studies have shown that fatty acids stimulate mitophagy (reviewed in 37); however, the mechanisms mediating these effects were not fully resolved. An important mechanism by which AMPK maintains mitophagy involves the phosphorylation and activation of ULK1 (38–42). We find that S108A-KI mice have reduced phosphorylation of ULK1 in the liver when fed a HFD and in hepatocytes treated acutely with palmitate. These data indicate that fatty acids stimulate mitophagy through AMPKβ1 Ser108 and that reductions in liver mitochondrial function in HFD-fed S108A-KI mice may be due to impaired mitophagy. As ULK1 can phosphorylate AMPKβ1 Ser108 (12), we measured a downstream substrate of ULK1, ATG14, and found no changes with palmitate treatment, suggesting that ULK1 is unlikely directly activated by free fatty acids. The role of AMPK in regulating mitophagy is extremely complex (43) with several new molecular mechanisms emerging, including an initiation cue of Parkin phosphorylation at Ser108 (42), mitoAMPK-mediated mitochondrial fission factor (MFF) phosphorylation (44), as well as several other signaling events which are beyond the scope of our work. Here, we show that LC3B-II flux is attenuated in mitochondrial enrichments from S108A-KI hepatocytes treated with palmitate, while no differences were found in the adaptor protein SQSTM1/P62 or other markers of mitophagy (BNIP3, NIX, and CISD1/MitoNEET). In addition to impairments in mitophagy, it is also possible that enlarged mitochondria may be a function of reduced mitochondrial fission induced through AMPK phosphorylation of MFF (45, 46) or dynamin-related protein 1 (47). These data highlight the importance of AMPKβ1 Ser108 in promoting ULK1 phosphorylation and autophagy/mitophagy in response to increased fatty acid availability while also highlighting the complexity of the mitophagy response that requires further study.

The sequence surrounding Ser108 is relatively well conserved between AMPKβ1 and β2, and while both β1 Ser108 and β2 Ser108 can be phosphorylated by CaMKKβ in vitro, only AMPKβ1 Ser108 phosphorylation is detectable in both basal and H_2O_2-stimulated HEK293 cells (12). However, it is unclear whether β2 Ser108 is phosphorylated in tissues. Currently, there is no high-resolution structural information for β2-containing AMPK trimeric complexes bound to an allosteric drug and metabolite site-binding activator; thus, the molecular basis for differential requirements of Ser108 phosphorylation between β-isoforms remains elusive. A potential limitation of our findings is that human liver is primarily composed of AMPKβ2-containing heterotrimers (48–50) which are insensitive to acute allosteric activation by free fatty acids (2). Despite the selectivity of this response toward the β1-isoform, it is important to note that AMPKβ1-specific activation in humans is sufficient to increase liver AMPK activity and impart physiological effects (19, 21, 22). These data suggest that fatty acyl-CoAs may also be important for regulating liver lipid metabolism and mitochondrial homeostasis in humans; however, this will require further study in primary human hepatocytes. Furthermore, since AMPKβ1 is the predominant β isoform in most other cell types besides cardiac and skeletal muscles, these findings may have implications for other metabolic processes outside of the liver, which will require further study. For example, ketogenic diets and intermittent fasting increase free fatty acids, an effect associated with activation of AMPK, mitochondrial biogenesis, mitophagy, and consequential improvements in mitochondrial function in multiple tissues and cell types. Future studies examining whether these effects may be mediated through AMPKβ1 Ser108 will be important. Additional understanding of the importance of the AMPK Ser108 residue will also be important to inform further refinement of compounds to control tissue specificity, duration, and magnitude of AMPK activation.

Materials and Methods

AMPK Activity Assay. AMPK was immunoprecipitated from 30–100 μg lysates with 1 μg antibodies against α1 or α2 subunit with protein G Sepharose. Phosphotransferase activity of AMPK toward the AMARA peptide (AMARAASAAALARRR) was assayed using [γ-^{32}P] ATP (51). Isoform-specific AMPKα subunit antibodies were custom made for immunoprecipitation as previously described (52).

Immunoblotting. For immunoblotting, tissue homogenates were prepared in lysis buffer (50 mM HEPES pH 7.4, 150 mM NaCl, 100 mM NaF, 10 mM Na-pyrophosphate, 5 mM EDTA, 250 mM sucrose, 1 mM DTT and 1 mM Na-orthovanadate, 1% Triton X-100, and complete protease inhibitor cocktail (Roche)), denatured in 4× SDS or Laemmli sample buffer, separated by SDS-PAGE, and transferred to nitrocellulose or PVDF membrane. Membranes were blocked for 1 h in 20 mM tris (pH 7.6), 137 mM NaCl, and 0.1% (v/v) Tween-20 (TBST) containing 5% (w/v) skim milk or BSA. The membranes were incubated in primary antibody prepared in TBST containing 1–5% (w/v) BSA overnight at 4°C. The following antibodies were used: pAMPKα1/α2 T172 (CST, 2535), AMPKα1 (Millipore, 07-350), AMPKα2 (Millipore, 07-363), pAMPKβ1 S108 (CST, 4181, CST, 23021*nonspecific band), AMPKβ1/β2 (CST, 4150), AMPKβ1 (CST, 12063), AMPKγ1 (OriGene, TA300519), pACC S79 (CST, 3661), ACC (CST, 3676), OXPHOS (Abcam, ab110413), β-actin (CST, 5125), pULK1 S555 (CST, 5869), ULK1 (CST, 8054), LC3B (CST, 2775), pATG14 S29 (CST, 92340), ATG14 (CST, 96752), p62 (CST, 5114), VDAC (CST, 4661), GAPDH (CST, 2118), BNIP3 (CST, 3769), NIX (CST, 12396), and CISD1 (CST, 83775). Detection was performed using horseradish peroxidase-conjugated secondary antibodies and enhanced chemiluminescence reagent. OXPHOS samples were not boiled to avoid the degradation of complexes.

Animals. We generated a targeted germline KI mouse model (in collaboration with Taconic Biosciences GmbH) in which the codon in exon 2 for Ser108 of *Prkab1* was modified to encode nonphosphorylatable Ala (*SI Appendix*). All experiments were approved by the McMaster University Animal Ethics Committee (#16-12-41) and conducted under the Canadian guidelines for animal research or approved by the local Ethical Committee of the Canton of Vaud Switzerland and performed under license number 3247. All mice were maintained under controlled environmental conditions: 12/12-h light/dark cycle with lights on at 0700 h, group housing, enrichment provided, and at room temperature (22–23°C). Male mice were used for all in vivo experiments. For HFD-fed studies, mice were switched from a normal chow diet (Diet 8640, Harlan Teklad) to a HFD (60% calories from fat; D12492 Research Diets) at 8 wk of age, and tests were performed at indicated weeks.

Metabolic Measurements. Metabolic monitoring was performed in a Comprehensive Lab Animal Monitoring System (CLAMS; Columbus Instruments) at 12 wk of age for chow-fed mice and 18 wk of age for HFD-fed mice. For intralipid and AICAR challenges, mice were given 48 h to acclimatize to the system, were fasted overnight starting at 1900 h, and given access to food for 2 h at 0700 h before having food removed simultaneously with an oral gavage of saline vs. 10 ml/kg intralipid or intraperitoneal injection of saline vs. 500 mg/kg AICAR at 0900 h. The mean lipid oxidation rates were calculated using the formula (1.6946 * VO_2) – (1.7012 * VCO_2) over 4 h starting 1 h postgavage for intralipid and over 1 h starting 6 h postinjection for AICAR as previously described (2, 53). ipGTT were performed in 6 h-fasted (0700 h to 1300 h) mice at 24 wk of age (16 wk of HFD). Basal blood glucose values were measured via tail-nick using an Accu-Chek blood glucose monitor (Roche) prior to an i.p. injection of 2.0 g/kg and 0.8 g/kg dextrose for chow-fed and HFD-fed mice, respectively. Blood glucose values were then followed following the injection at indicated time points. Intraperitoneal insulin tolerance tests were performed similarly to ipGTT, with an administration of 1.2 U/kg insulin in place of dextrose in HFD-fed mice (17 wk of HFD). Intraperitoneal pyruvate tolerance tests were performed in 12-h fasted mice (1900 h to 0700 h) with 1.5 g/kg sodium pyruvate in HFD-fed mice (18 wk of HFD).

Primary Hepatocytes. Primary hepatocytes were isolated from 10 to 15 wk-old WT or S108A KI mice fed a normal chow diet. Once mice were anesthetized and at surgical plane, livers were perfused with a solution containing 500 μM EGTA followed by type IV collagenase (320 U/mL, Sigma, C5138). The livers were removed,

placed in warm William's Medium E, and gently teased apart with forceps. For plated experiments, cells were suspended in William's Medium E (10% FBS, 1% antibiotic-antimycotic, and 1% L-glutamine), plated to ~85% confluency, and left to adhere overnight. The following morning, the cells were washed with PBS and serum starved for 1–2 h prior to the start of the experiment.

For autophagic assessment by western blotting experiments, following serum starving, the cells were treated with media containing 1% BSA (fatty acid, endo-toxin-free Sigma catalog: A8806) ±500 µM sodium palmitate (freshly made) and 50 µM chloroquine as indicated for 0.5 or 4 h. The cells were washed with cold PBS and snap frozen in cell lysis buffer containing 50 mM HEPES, 150 mM NaCl, 100 mM NaF, 10 mM Na-pyrophosphate, 5 mM EDTA, 250 mM sucrose, 1 mM DTT, and 1 mM Na-orthovanadate, with 1% Triton X and 1 tablet/50 ml complete protease inhibitor cocktail (Roche) and stored at −80°C until future analysis for western blotting. For autophagic flux by tandem fluorescence experiments, the cells were suspended in William's Medium E (10% FBS, 1% antibiotic-antimycotic, and 1% L-glutamine), plated to ~70% confluency, and simultaneously transfected on culture slides for 24 h using the Premo™ Autophagy Tandem Sensor RFP-GFP-LC3B Kit (ThermoFisher Scientific, P36239) according to the manufacturer's instructions. The next day, the cells were washed with warm PBS and serum starved for 2 h prior to the start of the experiment. The cells were treated for 20 h. To end experiments, the cells were washed with room-temperature PBS and fixed for 10 min using 4% PFA before mounting with ProLong™ Gold Antifade with DAPI (ThermoFisher Scientific, P36931) and adding coverslips.

Tissue Processing and TEM. For TEM, liver tissue was fixed in 2% glutaraldehyde in 0.1 M sodium cacodylate buffer (pH 7.4) for at least 24 h. Thin sections were cut by a Leica UCT ultramicrotome and picked up on Cu grids. Sections were poststained with uranyl acetate and lead citrate. Preparation, fixing, and sectioning were performed by the electron microscopy group at McMaster University Medical Center. Electron micrographs were obtained at a direct magnification of 7500× in an AMT 4-megapixel CCD camera (Advanced Microscopy Techniques) mounted in a JEOL JEM 1200 EX TEMSCAN transmission electron microscope and operating at an accelerating voltage of 80 kV. For quantification purposes, the researcher was blinded and 20 images per sample were acquired by random sampling. The total mitochondrial number and surface area were analyzed by a blinded researcher using Image J (NIH) and tracing the outer membrane of each mitochondria using the freehand selection tool with a stylus (Wacom). Samples per animal were averaged to give the represented values.

Tissue Triglycerides. Liver lipids were extracted by an adapted Folch method to determine triglyceride levels (54). Tissues were chipped (30–50 mg), homogenized in 1 mL of 2:1 chloroform:methanol, and mixed end-over-end overnight at 4°C. Samples were spun at 4,500 g for 10 min at 4°C, 0.9% NaCl added, and vortexed before being spun down at the same settings above. 400 µL of the bottom fraction was freeze-dried and solubilized in 100% 2-propranol before being assayed using a colorimetric kit as per manufacturer's instructions (Cayman Chemicals, Triglyceride Kit).

RNA Isolation and Real-Time Quantitative PCR (RT-qPCR). Tissues were lysed in 1 mL TRIzol reagent (Invitrogen) using ceramic beads and a Precellys 24 homogenizer (Bertin Technologies). Samples were spun down for 10 min at 12,000 g at 4°C. 200 µL of chloroform was added and shaken vigorously before spinning samples again at same settings. Supernatant was placed in new tubes and an equal amount of 70% ethanol was added and then vortexed. Solutions were loaded onto RNeasy columns and manufacturer's instructions were followed (Qiagen). 2 ng/µL RNA was added to a first master mix with 0.5 mM dNTPs (Invitrogen) and 50 ng/µL random hexamers (Invitrogen). The solutions were heated to 65°C for 5 min and then cooled back to 4°C. A second master mix containing 50 units of SuperScript III, DTT, and 5x First-Strand Buffer (Invitrogen) was added and heated to 25°C for 5 min and then 50°C for 1 h. All Taqman primers were purchased from Invitrogen (*Ppargc1a*, Mm01208835_m1; *Cpt1a*, Mm01231183_m1; and *Actb*, Mm02619580_g1), and relative gene expression was calculated using ($2^{-\Delta\Delta Ct}$) method. Values were normalized and expressed as relative to the housekeeping gene *Actb*.

Mitochondrial Respiration. Mitochondrial respiration was measured by high-resolution respirometry (Oroboros Oxygraph-2 k, Innsbruck, Austria) at 37°C and room air-saturated oxygen tension. The mitochondrial isolation procedure was similar to that described previously (55). Isolated liver mitochondrial respiration

was performed in MIRO5 buffer containing EGTA (0.5 mM), MgCl$_2$·6H$_2$O (3 mM), K-lactobionate (60 mM), KH$_2$PO$_4$ (10 mM), HEPES (20 mM), sucrose (110 mM), and fatty acid-free BSA (1 g/L). The order of substrate addition was malate (0.5 mM), pyruvate (5 mM), ADP (1 mM), glutamate (5 mM), oligomycin (1.25 µM), FCCP (titration of 0.5 µM until maximal uncoupled respiration reached), succinate (10 mM), and then malonate (5 mM).

Autophagic Flux Analyses by Confocal Microscopy. Images were obtained via Olympus FLUOVIEW FV1000 confocal laser scanning microscope (Olympus Corporation, Tokyo, Japan) equipped with a 60× (NA 1.42) oil immersion objective (Olympus) and Olympus FLUOVIEW software (ver4.2a) with appropriate filter conditions for the Premo™ Autophagy Tandem Sensor RFP-GFP-LC3B Kit. Image acquisitions were performed in at least five randomly selected fields of view, and experiments were performed in duplicate, per condition. Image analysis was performed using Fiji open-source software based on ImageJ, using the JACoP plugin. In brief, all colocalization analysis images were processed equally to remove background without altering signal, prior to the calculation of Mander's coefficient. Mander's coefficient values were expressed as the inverse of the percentage of pixels from one channel (i.e., RFP) overlapping with another (i.e., GFP), with independent RFP signal representing the degradation of acid-sensitive GFP.

Mitochondrial Enrichment. Primary hepatocytes were treated as above for autophagic assessment by western blotting experiments, with the following modifications. Cells were rinsed with ice-cold PBS twice before the application of lysis buffer supplemented with protease inhibitor solution supplied in the Qproteome mitochondria isolation kit (Qiagen, 37612). The cells were scraped on ice, and duplicates from 6-well dishes were combined to ensure sufficient protein content. Manufacturer's instructions were followed to yield standard preparations for enriched mitochondria, and 30 µL of cell lysis buffer (listed above) was added immediately to resuspend the pellet. Following kit instructions, 400 µL of cytosolic protein fraction was added to four volumes of ice-cold acetone to concentrate samples before resuspending in 50 µL of cell lysis buffer.

Statistics. Values were reported as mean ± SEM throughout the manuscript. White circles are individual mice per group or technical replicates from 3 to 5 separate experiments. Data were graphed and analyzed in GraphPad Prism 9 software using two-tailed Student's *t* tests, two-way ANOVA with Tukey's posthoc analysis, or repeated-measures two-way ANOVA with Sidak's posthoc analysis, where appropriate. Statistical significance was accepted at $P < 0.05$. Raw data is available in the *SI Appendix* section.

Data, Materials, and Software Availability. All study data are included in the article and/or *SI Appendix*.

Author affiliations: [a]Centre for Metabolism Obesity and Diabetes Research, McMaster University, Hamilton ON L8N 3Z5, Canada; [b]Division of Endocrinology and Metabolism, Department of Medicine, McMaster University, Hamilton ON L8N 3Z5, Canada; [c]Nestlé Institute of Health Sciences, Nestlé Research, Société des Produits Nestlé S.A., Lausanne 1015, Switzerland; [d]Department of Pediatrics, Faculty of Health Sciences, McMaster University, Hamilton ON L8N 3Z5, Canada; [e]Novo Nordisk Foundation Center for Basic Metabolic Research, University of Copenhagen, Copenhagen 2200, Denmark; and [f]Department of Biochemistry and Biomedical Sciences, McMaster University, Hamilton ON L8N 3Z5, Canada

1. R. H. Unger, P. E. Scherer, Gluttony, sloth and the metabolic syndrome: A roadmap to lipotoxicity. *Trends Endocrinol. Metab.* **21**, 345–352 (2010).
2. S. L. Pinkosky *et al.*, Long-chain fatty acyl-CoA esters regulate metabolism via allosteric control of AMPK β1 isoforms. *Nat. Metab.* **2**, 873-881 (2020), 10.1038/s42255-020-0245-2.
3. J. E. Song *et al.*, Mitochondrial fission governed by drp1 regulates exogenous fatty acid usage and storage in hela cells. *Metabolites* **11**, 322 (2021).
4. N. Turner *et al.*, Excess lipid availability increases mitochondrial fatty acid oxidative capacity in muscle: Evidence against a role for reduced fatty acid oxidation in lipid-induced insulin resistance in rodents. *Diabetes* **56**, 2085–2092 (2007).
5. P. Garcia-Roves *et al.*, Raising plasma fatty acid concentration induces increased biogenesis of mitochondria in skeletal muscle. *Proc. Natl. Acad. Sci. U S A.* **104**, 10709–10713 (2007).
6. G. R. Steinberg, D. Carling, AMP-activated protein kinase: The current landscape for drug development. *Nat. Rev. Drug Discov.* **18**, 527–551 (2019).
7. N. Dzamko *et al.*, AMPK β1 deletion reduces appetite, preventing obesity and hepatic insulin resistance. *J. Biol. Chem.* **285**, 115–122 (2010).
8. G. R. Steinberg *et al.*, Whole body deletion of AMP-activated protein kinase β2 reduces muscle AMPK activity and exercise capacity. *J. Biol. Chem.* **285**, 37198–37209 (2010).
9. K. I. Mitchelhill *et al.*, Posttranslational modifications of the 5′-AMP-activated protein kinase β1 subunit. *J. Biol. Chem.* **272**, 24475–24479 (1997).
10. T. J. Iseli *et al.*, AMP-activated protein kinase B subunit tethers a and y subunits via Its C-terminal sequence (186–270). *J. Biol. Chem.* **280**, 13395–13400 (2005).
11. Y. Yan, X. E. Zhou, H. E. Xu, K. Melcher, Structure and physiological regulation of AMPK. *Int. J. Mol. Sci.* **19**, 3534 (2018).
12. T. A. Dite *et al.*, The autophagy initiator ULK1 sensitizes AMPK to allosteric drugs. *Nat. Commun.* **8**, 1–13 (2017).
13. J. S. Oakhill *et al.*, Subunit myristoylation is the gatekeeper for initiating metabolic stress sensing by AMP-activated protein kinase (AMPK). *Proc. Natl. Acad. Sci.* **107**, 19237–19241 (2010).
14. B. Xiao *et al.*, Structure of mammalian AMPK and its regulation by ADP. *Nature* **472**, 230–233 (2011).
15. S. A.Hawley, The ancient drug salicylate directly activates amp-activated protein kinase. *Science* **336**, 918–922 (2012).
16. M. J. Sanders *et al.*, Defining the mechanism of activation of AMP-activated protein kinase by the small molecule A-769662, a member of the thienopyridone family. *J. Biol. Chem.* **282**, 32539–32548 (2007).
17. B. Xiao *et al.*, Structural basis of AMPK regulation by small molecule activators. *Nat. Commun.* **4**, 1–10 (2013).
18. R. W. Myers *et al.*, Systemic pan-AMPK activator MK-8722 improves glucose homeostasis but induces cardiac hypertrophy. *Science* **357**, 507–511 (2017).
19. R. M. Esquejo *et al.*, Activation of liver AMPK with PF-06409577 corrects NAFLD and lowers cholesterol in rodent and primate preclinical models. *EBioMedicine* **31**, 122–132 (2018).
20. M. J. Sanders *et al.*, Natural (dihydro)phenanthrene plant compounds are direct activators of AMPK through its allosteric drug and metabolite binding site. *J. Biol. Chem.* **298**, 101852 (2022).
21. K. Cusi *et al.*, Efficacy and safety of PXL770, a direct AMP kinase activator, for the treatment of non-alcoholic fatty liver disease (STAMP-NAFLD): A randomised, double-blind, placebo-controlled, phase 2a study. *Lancet Gastroenterol. Hepatol.* **6**, 889–902 (2021).
22. P. Gluais-Dagorn *et al.*, Direct AMPK activation corrects NASH in rodents through metabolic effects and direct action on inflammation and fibrogenesis. *Hepatol. Commun.* **6**, 101–119 (2021).
23. S. A. Hawley *et al.*, Use of cells expressing γ subunit variants to identify diverse mechanisms of AMPK activation. *Cell Metab.* **11**, 554–565 (2010).
24. M. D. Fullerton *et al.*, Single phosphorylation sites in Acc1 and Acc2 regulate lipid homeostasis and the insulin-sensitizing effects of metformin. *Nat. Med.* **19**, 1649–1654 (2013).
25. S. Herzig, R. J. Shaw, AMPK: Guardian of metabolism and mitochondrial homeostasis. *Nat. Rev. Mol. Cell Biol.* **19**, 121–135 (2018).
26. H. M. O'Neill, G. P. Holloway, G. R. Steinberg, AMPK regulation of fatty acid metabolism and mitochondrial biogenesis: Implications for obesity. *Mol. Cell. Endocrinol.* **366**, 135–151 (2013).
27. G. A. Baselli *et al.*, Rare ATG7 genetic variants predispose patients to severe fatty liver disease. *J. Hepatol.* **77**, 596–606 (2022).
28. J. W. Scott *et al.*, Small molecule drug A-769662 and AMP synergistically activate naive AMPK independent of upstream kinase signaling. *Chem. Biol.* **21**, 619–627 (2014).
29. Y. Lee *et al.*, PPARα is necessary for the lipopenic action of hyperleptinemia on white adipose and liver tissue. *Proc. Natl. Acad. Sci. U.S.A.* **99**, 11848–11853 (2002).
30. J. Carabelli *et al.*, High fat diet-induced liver steatosis promotes an increase in liver mitochondrial biogenesis in response to hypoxia. *J. Cell. Mol. Med.* **15**, 1329–1338 (2011).
31. E. P. Mottillo *et al.*, Lack of adipocyte AMPK exacerbates insulin resistance and hepatic steatosis through Brown and Beige adipose tissue function. *Cell Metab.* **24**, 118–129 (2016).
32. H. M. O'Neill *et al.*, AMP-activated protein kinase (AMPK) β1β2 muscle null mice reveal an essential role for AMPK in maintaining mitochondrial content and glucose uptake during exercise. *Proc. Natl. Acad. Sci. U.S.A.* **108**, 16092–16097 (2011).
33. S. Galic *et al.*, Hematopoietic AMPK β1 reduces mouse adipose tissue macrophage inflammation and insulin resistance in obesity. *J. Clin. Invest.* **121**, 4903–4915 (2011).
34. C. M. Hasenour *et al.*, 5-Aminoimidazole-4-carboxamide-1-β-D-ribofuranoside (AICAR) effect on glucose production, but not energy metabolism, is independent of hepatic AMPK in vivo. *J. Biol. Chem.* **289**, 5950–5959 (2014).
35. J. L. Estall *et al.*, Sensitivity of lipid metabolism and insulin signaling to genetic alterations in hepatic peroxisome proliferator-activated receptor-γ coactivator-1α expression. *Diabetes* **58**, 1499–1508 (2009).
36. Y. Kupriyanova *et al.*, Early changes in hepatic energy metabolism and lipid content in recent-onset type 1 and 2 diabetes mellitus. *J. Hepatol.* **74**, 1028–1037 (2021).
37. T. Zhang, Q. Liu, W. Gao, S. A. Sehgal, H. Wu, The multifaceted regulation of mitophagy by endogenous metabolites. *Autophagy* **00**, 1–24 (2021).
38. D. F. Egan *et al.*, Phosphorylation of ULK1 (hATG1) by AMP-activated protein kinase connects energy sensing to mitophagy. *Science* **331**, 456–462 (2011).
39. J. Kim, M. Kundu, B. Viollet, K. Guan, AMPK and mTOR regulate autophagy through direct phosphorylation of Ulk1. *Nat. Cell Biol.* **13**, 132–141 (2011).
40. J. W. Lee, S. Park, Y. Takahashi, H. G. Wang, The association of AMPK with ULK1 regulates autophagy. *PLoS One* **5**, 1–9 (2010).
41. W. J. Lee *et al.*, AMPK activation increases fatty acid oxidation in skeletal muscle by activating PPARα and PGC-1. *Biochem. Biophys. Res. Commun.* **340**, 291–295 (2006).
42. C. M. Hung *et al.*, AMPK/ULK1-mediated phosphorylation of Parkin ACT domain mediates an early step in mitophagy. *Sci. Adv.* **7**, 1–15 (2021).
43. R. Iorio, G. Celenza, S. Petricca, Mitophagy: Molecular mechanisms, new concepts on parkin activation and the emerging role of ampk/ulk1 axis. *Cells* **11**, 1–25 (2022).
44. J. C. Drake *et al.*, Mitochondria-localized AMPK responds to local energetics and contributes to exercise and energetic stress-induced mitophagy. *Proc. Natl. Acad. Sci. U.S.A.* **118**, 1–10 (2021).
45. S. Ducommun *et al.*, Motif affinity and mass spectrometry proteomic approach for the discovery of cellular AMPK targets: Identification of mitochondrial fission factor as a new AMPK substrate. *Cell. Signal.* **27**, 978–988 (2015).
46. E. Q. Toyama *et al.*, AMP-activated protein kinase mediates mitochondrial fission in response to energy stress. *Science* **351**, 275–281 (2016).
47. L. Xie *et al.*, Drp1-dependent remodeling of mitochondrial morphology triggered by EBV-LMP1 increases cisplatin resistance. *Signal Transduct. Target. Ther.* **5**, 1–12 (2020).
48. R. J. Ford *et al.*, Metformin and salicylate synergistically activate liver AMPK, inhibit lipogenesis and improve insulin sensitivity. *Biochem. J.* **468**, 125–132 (2015).
49. X. Stephenne *et al.*, Metformin activates AMP-activated protein kinase in primary human hepatocytes by decreasing cellular energy status. *Diabetologia* **54**, 3101–3110 (2011).
50. J. Wu *et al.*, Chemoproteomic analysis of intertissue and interspecies isoform diversity of AMP-activated protein kinase (AMPK). *J. Biol. Chem.* **288**, 35904–35912 (2013).
51. S. Ducommun *et al.*, Enhanced activation of cellular AMPK by dual-small molecule treatment: AICAR and A769662. *Am. J. Physiol. Endocrinol. Metab.* **306**, E688–96 (2014).
52. L. Bultot *et al.*, Benzimidazole derivative small-molecule 991 enhances AMPK activity and glucose uptake induced by AICAR or contraction in skeletal muscle. *Am. J. Physiol. Endocrinol. Metab.* **311**, E706–E719 (2016).
53. H. M. O. O'Neill *et al.*, AMPK phosphorylation of ACC2 is required for skeletal muscle fatty acid oxidation and insulin sensitivity in mice. *Diabetologia* **57**, 1693–1702 (2014).
54. J. Folch, M. Lees, G. H. Sloane Stanley, A simple method for the isolation and purification of total lipides from animal tissues. *J. Biol. Chem.* **226**, 497–509 (1957).
55. B. K. Smith *et al.*, Salsalate (salicylate) uncouples mitochondria, improves glucose homeostasis, and reduces liver lipids independent of ampk-β1. *Diabetes* **65**, 3352–3361 (2016).